Journal of Magnetic Resonance **147,** 217–225 (2000)
doi:10.1006/jmre.2000.2196, available online at http://www.idealibrary.com on IDEAL®

Magic-Angle Sample Spinning Electron Paramagnetic Resonance—Instrumentation, Performance, and Limitations

Dirk Hessinger, Christian Bauer, Michael Hubrich, Gunnar Jeschke, and Hans-Wolfgang Spiess

Max-Planck-Institut für Polymerforschung, Postfach 3148, 55028 Mainz, Germany

Received March 29, 2000; revised August 21, 2000

An electron paramagnetic resonance (EPR) setup for line narrowing experiments with fast sample spinning at variable angles between the rotation axis and the static magnetic field is described and applied in the magic-angle sample spinning (MAS) EPR experiment at X-band frequencies (9.5 GHz). Sample spinning speeds up to 17 kHz at temperatures down to 200 K can be achieved with rotors of 4-mm outer and 2.5-mm inner diameter without severe losses in microwave amplitude compared to standard pulse EPR probeheads. A phase cycle is introduced that provides pure absorption MAS EPR spectra and allows one to distinguish between positive and negative frequency offsets (pseudo-quadrature detection). Possible broadening mechanisms in MAS EPR spectra are discussed. It is demonstrated both by theory and by experiment that the MAS EPR experiment requires excitation bandwidths that are comparable to the total spectral width, since otherwise destructive interference between contributions of spins with similar resonance offsets suppresses the signal. Experimental observations on the E_1' center in γ-irradiated silica glass and on the SO_3^- radical in γ-irradiated sulfamic acid are reported.

Key Words: **pulse EPR; MAS; high resolution; solid state; resonator.**

INTRODUCTION

Magnetic resonance spectra of species in the solid state or of slowly tumbling molecules are often strongly broadened due to the anisotropy of magnetic interactions. The magic-angle sample spinning (MAS) technique (*1, 2*) has become the most widespread approach for obtaining high-resolution NMR spectra in such situations. In its most popular form the experiment is based on observing a train of rotational echoes whose amplitudes are modulated only by isotropic interactions. Fourier transformation (FT) of the echo train yields a spectrum consisting of the isotropic lines and, if the anisotropy is larger than the rotation frequency, of sidebands that are offset by integer multiples of the rotation frequency (*3*). Unfortunately, this approach requires rotation frequencies that are larger or at least comparable with the width of the spectrum (*4*). As electron paramagnetic resonance (EPR) spectra typically cover tens of megahertz or even more, application of this MAS experiment in EPR is impossible. On the other hand, state-of-the-art sample spinning systems achieve rotation frequencies of up to 35 kHz which are comparable to $1/T_1$ for electron spins in many systems. Averaging of anisotropic interactions on the time scale of longitudinal relaxation has been applied in NMR in the magic-angle hopping (*5*) and magic-angle turning (*6*) experiments for correlating the isotropic spectrum to the static spectrum. This offers a route for artificial narrowing of EPR lines through MAS. We have recently shown that the magic-angle turning experiment can be adapted to EPR spectroscopy (*7*), applying 15 to 20-kHz MAS to yield narrowed isotropic lines. In this work we describe the MAS EPR probehead and introduce an improved version of the experiment that provides pure absorption spectra. Furthermore, technical limitations of the experiment are considered that may lead to spectral broadening or a decrease in sensitivity. It is shown that the experiment depends critically on the ratio between excitation bandwidth and anisotropy. Experimental spectra are presented for E_1' centers in γ-irradiated silica glass and SO_3^- radicals in γ-irradiated sulfamic acid.

INSTRUMENTATION

Combination of the Stator–Rotor System with a Microwave Resonator

At least two-thirds of a sample rotation must be completed on the time scale of T_1 to make the magic-angle turning experiment feasible (see Theory below). This requires rotation frequencies above 10 kHz as they are available with current high-speed MAS NMR rotor/stator systems. Two commercial systems (Bruker, Rheinstetten, Germany) with rotors of outer diameter of 4 and 2.5 mm and maximum rotation frequencies ν_{rot} of 17 and 35 kHz were tested. To keep dielectric losses in the rotor material (zircon dioxide ceramics) to a minimum, the stator was fitted with a dielectric resonator (see Fig. 1a). The sapphire dielectric ring (outer diameter 8 mm, inner diameter 5 mm, length 9 mm), which can be supplemented with an ENDOR coil, is contained in a Teflon shell that in turn fits into the outer resonator made of brass (see Fig. 1b). This whole structure fits into the commercial stator instead of the NMR coil. The bottom of the cylindrical outer resonator (TE_{011}, inner

1090-7807/00 $35.00

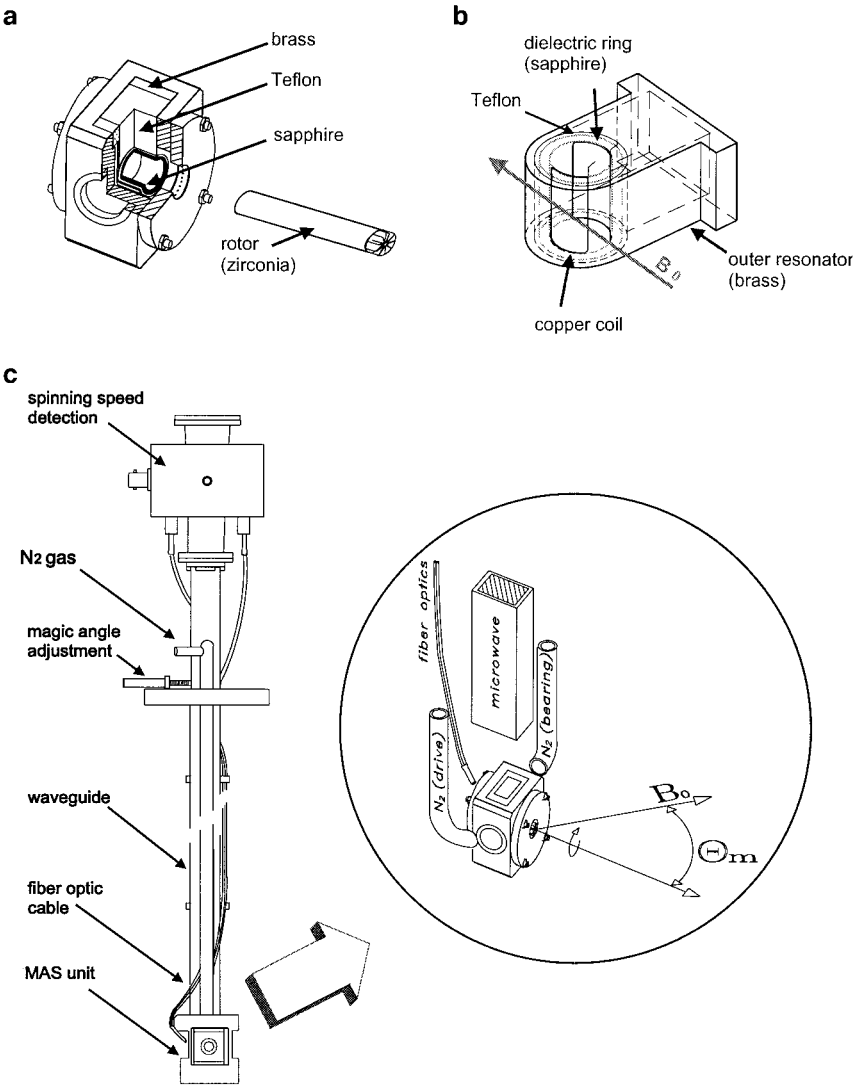

FIG. 1. Probehead for fast sample spinning at variable angles with respect to the magnetic field. (a) Combination of the resonator block with a commercial MAS NMR stator/rotor system (Bruker). (b) Dielectric resonator with brass outer resonator and optional ENDOR coil. (c) View of the complete probehead.

diameter and length 9 mm) is made of a removable grid of brass wires. A metal part with a bearing gas outlet on the bottom of the commercial MAS stator had to be replaced with a similarly shaped rexolite part to improve resonator quality. The bearing outlet was also decreased in size to facilitate rotation in a horizontal position. In addition, this part features an opening for optical detection of the rotation frequency. The top brass plate is removable for insertion of the rotor and has a center hole for rotor repositioning during the start of rotation (see below). The distance of this plate to the rotor cap can be adjusted by 2–3 mm to obtain the desired resonance frequency.

In the case of 4-mm rotors, the dimensions are similar to dielectric resonators for conventional EPR tubes, except for the thicker walls of the rotor (inner diameter 2.5 mm) compared to an EPR tube. Note that to the microwave (mw), the rotor itself appears like another dielectric ring resonator; which must be considered when adjusting the resonance frequency. Despite the compromises in resonator design that had to be made, we obtain a maximum Q_L of 660 which is more than sufficient for pulse EPR. The optimum quality factor for pulse EPR is determined by a compromise between the decrease in the mw field strength B_1 at given incident mw power and the increase in resonator bandwidth with decreasing Q_L (*8*). For the mw power currently available on our spectrometer we estimate that the optimum Q_L is close to 200. The quality factor is not significantly influenced by the sample material inside the rotor, hence the coupling can be adjusted once and for all during probehead design. The 2.5-mm rotors are not so well suited to X-band frequencies. In this case we obtain only $Q_L < 100$, which is less than optimum.

Sample Rotation and Rotation Axis Adjustment

Fast sample rotation in EPR is needed not only for the MAS experiment, but also for the application of experiments like anisotropy-resolved EPR (*9*, *10*) to organic radicals. As such experiments are most efficient and most easily analyzed for right-angle rotation, it is desirable to have a probehead with an adjustable angle between the rotation axis and the axis of the static field. This can be conveniently realized for a horizontal rotation axis, because the static field is also horizontal in standard EPR spectrometers. The angle between the rotation axis and static field can then be varied simply by turning the whole probehead about its vertical long axis (see Fig. 1c). A micrometer screw allows for fine adjustment. The circular top plate of the probehead can be mounted on the cryostat of the Bruker ESP 380E spectrometer (Oxford). A semi-rigid cable is used to connect the mw bridge to the waveguide (brass) which is filled with rexolite (Goodfellow). Because of the higher dielectric constant ($\epsilon \sim 2.5$) compared to air, this reduces the size of the waveguide to Ku-band dimensions (15.8 × 7.9 mm). Thereby enough space inside the cryostat is retained for the glass tubing for the drive and bearing gas of the rotor system.

We found that the horizontal position of the rotor sometimes led to instabilities during the start of rotation resulting in ejection of the rotor from the stator. This problem can be overcome by shooting the rotor back into the stator with a short pulse of pressured air. This can be achieved in the presence of moderate bearing and drive pressure, so that the rotor is stabilized by the rotation. Thin Teflon tubing (inner diameter 0.5 mm) is used to provide the pressured air to an inlet in the top brass plate of the resonator.

Even organic radicals and point defects in crystals often have relaxation times at ambient temperature that would lead to substantial signal loss during the 20–40 μs required for the MAS experiment at ν_{rot} = 17–30 kHz. Sample cooling often leads to a significant increase in T_1. We achieved stable rotation for sample temperatures down to 200 K if nitrogen was used as the drive and bearing gas. Pressure control for drive and bearing as well as the variable temperature unit was adapted from commercial hardware for MAS NMR experiments (Bruker). Typical working pressures are 3 bar for the bearing and 2.4 bar for the drive gas at ν_{rot} = 17 kHz.

The whole setup with 4-mm rotors provides rotation frequencies up to 17 kHz at temperatures down to 200 K and mw $\pi/2$ pulse lengths down to $t_{\pi/2}$ = 24 ns, which is 1.5 times longer than mw $\pi/2$ pulses in a commercial dielectric resonator overcoupled to the same Q_L value. The setup with 2.5 mm achieves $\nu_{rot} \leq 30$ kHz and $t_{\pi/2} \geq 64$ ns. This setup was only tested at ambient temperature.

THEORY

Basics of MAS EPR

Consider first an anisotropic interaction whose orientation dependence can be described by a second-rank tensor **G** with principal values G_{xx}, G_{yy}, and G_{zz}. Note that such a treatment can be applied to any line of a hyperfine multiplet with **G** being a sum of the tensor which describes the electron Zeeman interaction and of the hyperfine tensors multiplied by the appropriate nuclear magnetic quantum numbers. Expansion of the tensor **G** into irreducible spherical tensor operators reveals that a rotation of the sample with angular frequency ω_r about an arbitrary axis leads to a time-dependent interaction frequency (secular part)

$$\begin{aligned}\omega_G(t) = {} & C_0(\alpha, \beta, \theta) + C_1(\alpha, \beta, \theta)\cos(\omega_r t + \gamma) \\ & + S_1(\alpha, \beta, \theta)\sin(\omega_r t + \gamma) \\ & + C_2(\alpha, \beta, \theta)\cos(2\omega_r t + 2\gamma) \\ & + S_2(\alpha, \beta, \theta)\sin(2\omega_r t + 2\gamma), \end{aligned} \quad [1]$$

where α, β, and γ are Euler angles that characterize the relative orientation of the rotor fixed frame to the principal axis system of **G**, and θ is the angle between the rotation axis and the static field direction (*11*, *12*). In particular, with the isotropic part

$$G_{iso} = \frac{1}{3}(G_{xx} + G_{yy} + G_{zz}), \quad [2]$$

the anisotropy

$$\Delta_G = G_{zz} - G_{iso}, \quad [3]$$

and the asymmetry

$$\eta_G = \frac{G_{yy} - G_{xx}}{\Delta_G} \quad [4]$$

of the interaction, the time-independent part is expressed by

$$\begin{aligned} C_0 = {} & G_{iso} + \Delta_G \frac{3\cos^2\theta - 1}{2} \\ & \times \left[\frac{3\cos\beta - 1}{2} - \frac{\eta_G}{2}\cos(2\alpha)\sin^2\beta\right]. \end{aligned} \quad [5]$$

For the magic angle, $\theta_m = \arccos\sqrt{1/3} \approx 54.7°$, one finds $C_0 = G_{iso}$, so that a highly resolved isotropic spectrum can be obtained by averaging the time-dependent parts. To achieve this, it is sufficient to measure ω_G at three rotor positions spaced by two 120° intervals, as was first realized by Bax *et al.* (*5*). This can be easily checked by substituting γ_0, $\gamma_0 + 120°$,

and $\gamma_0 + 240°$ for γ in Eq. [1] and computing the average of the three values for ω_G. This experiment was first done in NMR with jump reorientation of the sample (magic-angle hopping), which could not be realized at sufficiently fast time scales for EPR. A later version by Gan (*6*) used "ultraslow" rotation for the sample reorientation. This so-called magic-angle turning experiment is based on the fact that for most samples the time required for a frequency measurement of sufficient precision is so short that the rotation frequency can be chosen low enough for reorientation effects to be negligible during the frequency measurements at the three sample positions.

The MAS EPR experiment introduced by Hubrich *et al.* (*7*) adapts this idea to the usual experimental situation in pulse EPR where uniform excitation of the whole spectrum is usually impossible because of excitation bandwidth restrictions and free induction decays are unobservable because of instrumental dead time t_d (Fig. 2). The experiment starts by generation of electron coherence at rotor phase γ_0 by an mw $\pi/2$ pulse. The coherence evolves freely for time $t/3$ with frequency $\omega_G(\gamma_0)$ and is then stored as polarization by the second mw $\pi/2$ pulse. Half of the magnetization is lost at this point, because coherence with the same phase as the mw pulse is unaffected and decays with relaxation time T_2. The polarization remains apart from decaying with relaxation time T_1, i.e., most of it survives a reorientation by 120°. After the time T required for this reorientation, the polarization is again transferred to coherence by an mw $\pi/2$ pulse and evolves for time $t/3$ with frequency $\omega_G(\gamma_0 + 120°)$. Storage of the magnetization as polarization and sample reorientation are repeated; again half of the remaining magnetization is lost. At the third position, the polarization is again transferred to coherence by an mw $\pi/2$ pulse and evolves freely for a time $\tau > t_d$, after which a refocusing mw π pulse is applied to overcome the inevitable dead time of the receiver. Echoes are observed at times $\tau - t/3$ and $\tau + t/3$ after the π pulse. Because evolution during the intervals of length τ is rephased by the π pulse, this amounts to a net evolution for another interval of length $t/3$ with frequency $\omega_G(\gamma_0 + 240°)$ for the second echo.

The phase gained by the evolution at all three rotor positions is given by

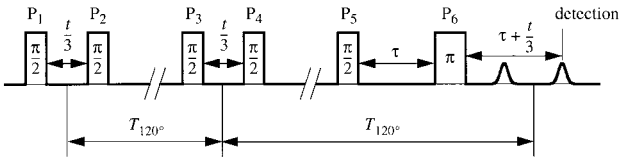

FIG. 2. Pulse sequence for the MAS EPR experiment. The variation of the amplitude of the second echo is observed as a function of time t. The phase cycle is given in Table 1.

TABLE 1
Phase Cycle for Constructing a Quadrature Phase-Modulated Signal in the MAS EPR Experiment (see Fig. 3)

P_2	P_4	P_5	P_6	Detection	Part
$-x$	$-x$	$+y$	$+x$	$+x$	Real
$+y$	$-y$	$+y$	$+x$	$+x$	Real
$+y$	$-x$	$+x$	$+y$	$+x$	Real
$-x$	$+y$	$+x$	$+y$	$+x$	Real
$-y$	$-x$	$+y$	$+x$	$+x$	Imaginary
$-x$	$-y$	$+y$	$+x$	$+x$	Imaginary
$-x$	$-x$	$+x$	$+y$	$+x$	Imaginary
$+y$	$-y$	$+x$	$+y$	$+x$	Imaginary

Note. The pulses not contained in the table have phase $+x$. To avoid distortions by an echo crossing, signals of the same experiments with inverted phase ($-x$) of the first mw pulse (P_1) have to be subtracted.

$$\phi_{iso} = \phi_1 + \phi_2 + \phi_3 = \omega_G(\gamma_0)\,\frac{t}{3} + \omega_G(\gamma_0 + 120°)\,\frac{t}{3} + \omega_G(\gamma_0 + 240°)\,\frac{t}{3} = G_{iso}t \qquad [6]$$

for rotation at the magic angle. To observe this phase variation in the echo amplitude on varying time t, it is not sufficient to store only coherence along one axis of the rotating frame with the second and fourth $\pi/2$ pulse. A phase cycle has to be devised that combines the sines and cosines of the phases ϕ_1, ϕ_2, and ϕ_3 to obtain the expressions for $\cos(\phi_1 + \phi_2 + \phi_3)$ and $\sin(\phi_1 + \phi_2 + \phi_3)$ for the real and imaginary part of a complex-valued time-domain signal, respectively. Trigonometric relations reveal that four phase cycle steps are necessary for each of the two signal components. The necessary phase cycling of the fifth $\pi/2$ pulse corresponds to another loss of half the magnetization, hence only 12.5% of the thermal equilibrium magnetization contributes to the observed signal. This loss is not specific to the EPR case; it also occurs in the magic-angle turning NMR experiment (*6*). The complete phase cycle is given in Table 1. To avoid echo crossings, it has to be combined with a phase cycle $[+x, -x]$ of the first pulse and subtraction of the corresponding signals to give a 16-step cycle. Such cycling of the first pulse does not lead to further signal loss. FT of the time-domain signal with respect to t yields the isotropic EPR spectrum. Acquisition of a complex time-domain data set ensures that positive and negative frequency offsets from the excitation position can be distinguished in this spectrum (*11, 12*). This also holds true for cases where the EPR frequencies are determined by several anisotropic interactions as long as only secular terms in the Hamiltonian need to be considered.

Broadening Mechanisms and Sensitivity

In the idealized experiment described above, linewidths in MAS EPR spectra are determined by transverse relaxation

(T_2). Additional broadening is expected if the reorientation of the sample during the intervals of length $t/3$ can no longer be neglected for the maximum t. For utmost resolution $t_{max} > 3T_2$ should be used, which may be long enough for such broadening to be observable at typical T_2 of about 1 μs. In practice, lines in an ideal isotropic EPR spectrum may, however, be significantly broader than suggested by T_2 because of unresolved isotropic hyperfine couplings, and, especially in disordered systems like polymers, glasses, and frozen solutions, a distribution of isotropic g values and hyperfine couplings (g and hyperfine strain). MAS is also unable to completely remove anisotropic broadening in cases where the secular approximation breaks down, as is, for instance, the case for many quadrupole nuclei in NMR (*13*). This situation is often met in EPR for hyperfine couplings with protons or nitrogen nuclei. Our model calculations show that it is significant only rather close to the exact cancellation condition where twice the nuclear Zeeman frequency matches the hyperfine coupling, as, for instance, for α- and β-protons in aliphatic organic radicals (data not shown). Finally, broadening may be due to a mismatch of the angle between the rotation axis and static field direction. In this case, part of the anisotropy contributes to C_0 (Eq. [1]) and is not averaged.

Sensitivity of MAS EPR is limited not only by the loss of 87.5% of the thermal equilibrium magnetization in the storing and recalling during the pulse sequence, but also by longitudinal relaxation during the reorientation intervals. Two-thirds of a sample rotation have to be completed in these intervals, which requires a time between 20 and 40 μs at the rotation frequencies achieved with our setup. Even at the lowest temperature of 200 K for which we can perform the experiment, this can still lead to significant loss of magnetization for organic radicals and point defects in crystals. Most transition metal ions are not accessible to our experiment so far, because neither their T_1 nor their T_2 values are long enough at such temperatures. However, note that pulse EPR experiments at temperatures as high as 200 K have been performed on several Cr(V) complexes (*14*).

Spectral diffusion may also cause a loss of signal. Furthermore, part of the magnetization transfer due to spectral diffusion is to spin packets with only a slightly different orientation. This may lead to incomplete refocusing of the anisotropy of the interactions and thus to some line broadening in the MAS EPR spectra. For these reasons it is important to work at temperatures where molecular reorientation on the time scale of the experiment can be neglected and, if possible, at concentrations where spin diffusion is not relevant.

Incomplete Excitation

Spectral widths usually exceed the excitation bandwidth in pulse EPR, quite often even by a large factor. A given initial orientation of the paramagnetic center only contributes to the MAS signal provided that the electron spins can be excited at all three rotor positions during the experiment. If this is achieved only for a small part of all initial orientations, the signal amplitude is reduced, but narrow EPR spectra are still expected, because the averaging of anisotropic interactions is complete even for a single initial orientation. Incomplete excitation is, however, expected to lead to substantial sensitivity loss if the spectral width exceeds the excitation bandwidth by a factor of 5 or more, because the fraction of contributing initial orientations then becomes very small. It is also not immediately clear from the EPR spectrum where the optimum position for excitation is, so that in this situation MAS EPR must be performed at several observer fields. Nevertheless, it should still be possible to apply MAS EPR to a substantial number of organic radicals and point defects.

This simplified view, unfortunately, does not include interference effects due to the phase dispersion of the magnetization that is excited off resonance. Indeed, in our experiments we did not obtain MAS EPR spectra for a number of radicals for which estimates suggested that the fraction of contributing orientations was still substantial and for which we had obtained a rotational echo after a 360° reorientation. To clarify this point, we further analyzed the experiment for nonideal pulses with the rotating-frame Hamiltonian

$$\mathcal{H}_{+x} = \omega_1(rS_z + S_x), \qquad [7]$$

for a pulse along $+x$, where ω_1 is the pulse amplitude in angular frequencies and r characterizes the resonance offset as a fraction or multiple of ω_1. This Hamiltonian is diagonalized by the unitary transformation $U = \exp\{-i\theta_r S_y\}$ with $\theta_r = \mathrm{atan}(r/q)$ and $q = \sqrt{1 + r^2}$. Straightforward application of the product operator formalism yields for the real and imaginary part of the time-domain data obtained with the above-mentioned phase cycle

$$\mathrm{Re}(V) = D_1(r_0) \cdot D_1(r_{120}) \cdot E_1(r_{240}) \cdot \cos(\omega_{iso}t) - D_2(r_0) \cdot D_2(r_{120}) \cdot E_2(r_{240}) \cdot \sin(\omega_{iso}t), \qquad [8]$$

$$\mathrm{Im}(V) = D_1(r_0) \cdot D_1(r_{120}) \cdot E_1(r_{240}) \cdot \sin(\omega_{iso}t) - D_2(r_0) \cdot D_2(r_{120}) \cdot E_2(r_{240}) \cdot \cos(\omega_{iso}t), \qquad [9]$$

where the factors D_1 and D_2 characterize the dependence of in-phase and out-of-phase components excited and detected by a pair of two $\pi/2$ pulses on the resonance offset and E_1 and E_2 are analogous factors for the final $\pi/2$–π pulse pair. The normalized resonance offsets r_0, r_{120}, and r_{240} correspond to the three rotor positions and depend on ω_G. The off-resonance factors are given by

$$D_1(r) = \frac{2}{q^4}\sin^2\left(\frac{\pi}{4}q\right)\left[1 + (2r^2 + 1)\cos\left(\frac{\pi}{2}q\right)\right], \qquad [10]$$

$$D_2(r) = \frac{r}{q^3}\left[\sin(\pi q) - 2\sin\left(\frac{\pi}{2}q\right)\right], \quad [11]$$

$$E_1(r) = -\frac{1}{q^3}\sin\left(\frac{\pi}{2}q\right)\left[r^2 - 2r^2\cos\left(\frac{\pi}{2}q\right) + (2r^2+1)\cos(\pi q)\right], \quad [12]$$

and

$$D_2(r) = \frac{2r}{q^4}\sin^2\left(\frac{\pi}{4}q\right)\left[2 + r^2 + 2q^2\cos\left(\frac{\pi}{2}q\right) + (1+2r^2)\cos(\pi q)\right]. \quad [13]$$

For $r \to 0$, D_1 and E_1 approach unity, while D_2 and E_2 approach zero. After averaging over the Euler angles, the result depends only on the excitation position, the ratio ω_1/Δ_G, and slightly on the asymmetry parameter η_G. Similar but somewhat more lengthy formulas can be obtained for arbitrary flip angles of the pulses.

Numerical simulations show that for $\omega_1/\Delta_G > 2$, 90% or more of the maximum intensity is obtained. For $\omega_1/\Delta_G < 2$, however, the absolute value of the intensity drops considerably, but an amplitude above 10% is still observed for $\omega_1/\Delta_G > 0.25$ (Fig. 3a). With decreasing ratio ω_1/Δ_G we also find that the phase of the magnetization in the detection period varies more strongly with the offset of the observer position from the isotropic frequency (field), as can be seen in Figs. 3b–3g. As there always is a distribution of the isotropic frequency due to relaxational broadening, unresolved isotropic hyperfine couplings, and strain, this leads to destructive interference. As a consequence, MAS EPR experiments may fail also for $\omega_1/\Delta_G > 0.25$, depending on the natural linewidth in the isotropic spectrum. For an anisotropy for the **g** tensor as in the E_1' center in silica glass, the signal is expected to vanish already at $\omega_1/\Delta_G = 0.463$ for a natural linewidth of about 1 MHz, as can be seen in Fig. 3g.

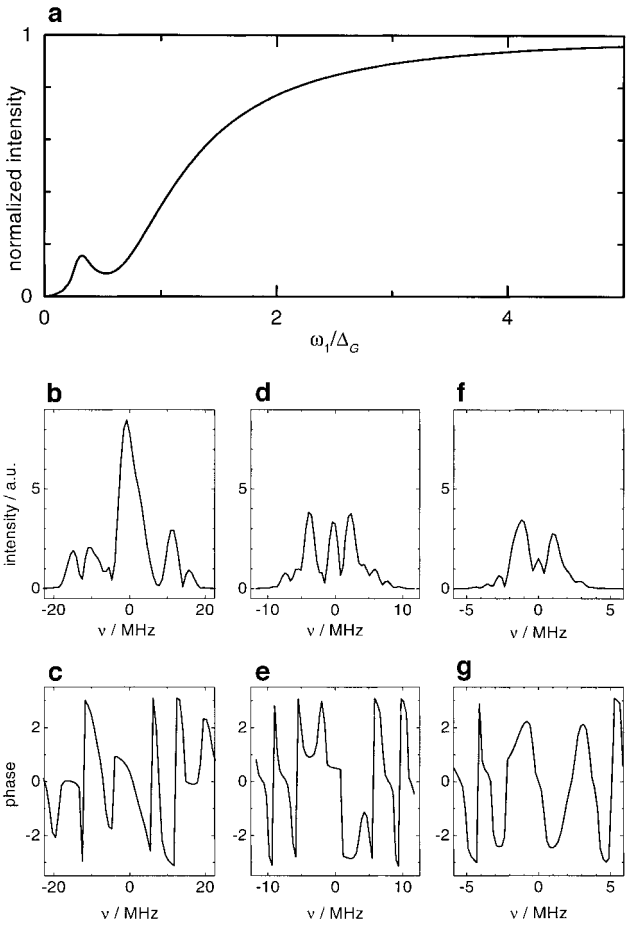

FIG. 3. Effects of incomplete excitation on MAS EPR signals (simulations). (a) Normalized intensity I_n of the MAS EPR signal for an axial tensor ($\eta_G = 0$) plotted against the ratio ω_1/Δ_G between mw amplitude and anisotropy of the interaction. (b–f) Total signal intensity and phase as a function of the offset ν of the observer position from the isotropic frequency. The assumed anisotropy Δ_G corresponds to the g tensor of the E_1' center in γ-irradiated silica glass. (b, c) $\omega_1/\Delta_G = 1.851$. (d, e) $\omega_1/\Delta_G = 0.926$. (f, g) $\omega_1/\Delta_G = 0.463$.

EXPERIMENTAL RESULTS

All MAS EPR experiments were performed on a Bruker ESP 380E spectrometer at frequencies of about 9.5 GHz with the setup described in the instrumentation section. EPR spectra of the test samples have been measured on the Bruker ESP 380E (X-band) and Elexsys 680 (W-band) spectrum with commercial standard probeheads.

γ-Irradiated Silica Glass

The E_1' center in γ-irradiated quartz or silica glass is a convenient model system for time-domain EPR experiments (*8*) because of the small width of its spectrum (about 0.3 mT at X-band frequencies) (*15*) and the long relaxation times T_1 (~200 μs) and T_2 (~24 μs) (*16*). In our own sample obtained by γ-irradiation of Suprasil glass, we observe a phase memory time $T_m = 6.3$ μs because of instantaneous diffusion effects at the applied pulse lengths. The real and imaginary parts of the MAS EPR signal for this sample (ambient temperature) are shown in Figs. 4a and 4b. The signal decays in a time that is significantly shorter than that suggested by the value of T_m. Complex FT with subsequent phase correction yields the absorption and dispersion spectrum in Figs. 4c and 4d. The frequency of the signal is in agreement with the expected isotropic g value of 2.0009 (*15*). The full width at half height of the line in the pure absorption spectrum is 1.4 MHz, which is by a factor of 0.7 smaller than in our previous absolute-value spectrum (*7*). This is in reasonable agreement with the expected narrowing factor $1/\sqrt{3} \sim 0.58$. However, according to the phase memory time, a linewidth of only 50 kHz would be

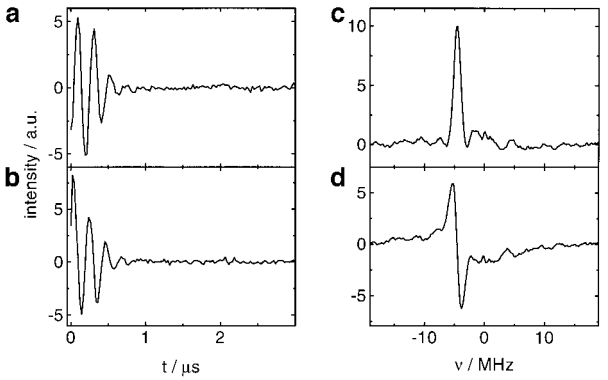

FIG. 4. MAS EPR on the E_1' center in γ-irradiated silica glass (B_0 = 331.76 mT, ν_{mw} = 9.285 GHz, ν_{rot} = 17 kHz, $t_{\pi/2}$ = 32 ns). (a) Real part and (b) imaginary part of the time-domain signal. (c) Absorption and (d) dispersion spectrum obtained by FT of the complex time-domain signal.

expected. None of the broadening mechanisms discussed above is expected to contribute significantly to the observed linewidth and some further possibilities for instrumental contributions have been excluded before (*7*). In this publication, the discrepancy was attributed to *g* strain in the glassy material. The echo-detected W-band EPR spectrum of the sample taken at 94.2 GHz (Fig. 5a) also exhibits a strong discrepancy between the linewidth of the singularities expected from T_m and observed experimentally and thus supports our previous interpretation.

According to the considerations under Theory, such strain

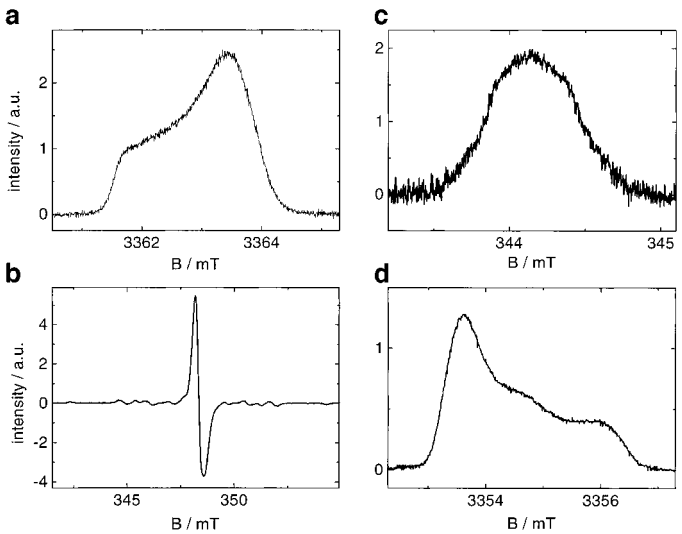

FIG. 5. EPR spectra of the test samples. (a) Echo-detected EPR spectrum of the E_1' center in γ-irradiated silica glass measured at W-band (94.159 GHz). (b) CW EPR of γ-irradiated sulfamic acid at X-band (9.7719 GHz). The strong line in the center is due to the SO_3^- anion radical; the weaker lines belong to the neutral NH_2-SO_3 radical. (c) Echo-detected EPR spectrum of the SO_3^- anion radical in γ-irradiated sulfamic acid at X-band (9.649 GHz). (d) Echo-detected EPR spectrum of the SO_3^- anion radical in γ-irradiated sulfamic acid at W-band (94.039 GHz).

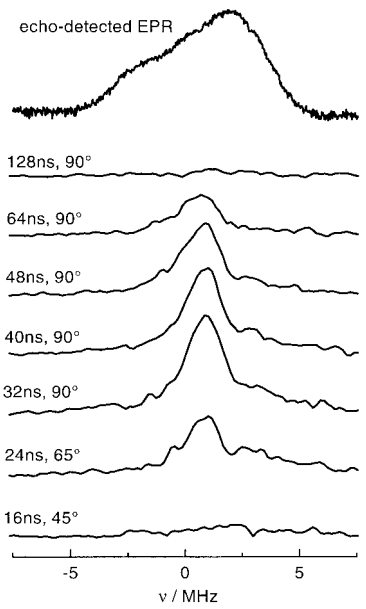

FIG. 6. Dependence of the MAS EPR spectrum of the E_1' center in γ-irradiated silica glass on excitation bandwidth and flip angle. An echo-detected EPR spectrum is shown for comparison. The labels on the traces designate the length and actual flip angle of the nominal π/2 pulses (B_0 ~ 331.9 mT, ν_{mw} = 9.2932 GHz, ν_{rot} = 17 kHz). All spectra are absolute-value spectra and are referenced to the same observer *g* value.

broadening should lead to destructive interference of the MAS EPR signal at excitation bandwidths below the spectral width. This was tested by deliberately reducing mw power and thus excitation bandwidth (Fig. 6, note that absolute-value spectra are shown here). The optimum is obtained for $t_{\pi/2}$ = 32 ns. Significant signal loss is observed already for $t_{\pi/2}$ as short as 48 ns; at a pulse length of 128 ns no MAS EPR signal can be observed. This would suggest that with our present setup MAS EPR can only be applied to species with spectral widths up to about 20 MHz (0.7 mT), assuming that the relative broadening in the isotropic EPR spectra is similar. Such an estimate is in good agreement with our experience. Note, however, that mw π/2 pulse lengths down to 3.6 ns have been reported recently (*17*). Even allowing for an increase of the pulse length by a factor of 2 in an MAS setup, which is worse than in our case, this would extend the accessible spectral widths up to 3 mT.

We also checked the possibility of extending excitation bandwidth by using shorter pulses with smaller flip angles. For flip angles of 65° for the nominal π/2 pulses signal loss is still tolerable, and such settings may be favorable in some cases. Reducing the flip angles by a factor of 2, however, leads to virtually complete signal loss in this six-pulse sequence; see lower traces in Fig. 6.

γ-Irradiated Sulfamic Acid

To test our proposition that species with spectral widths of about 0.7 mT should still yield artificially narrowed MAS EPR

signals, we performed experiments on the SO_3^- anion radical center found in γ-irradiated sulfamic acid (systematic name, amidosulfonic acid). The echo-detected X-band EPR spectrum of this sample is a structureless line of nearly Gaussian shape with full width at half height of about 0.64 mT (Fig. 5c). The broadening is due to unresolved hyperfine couplings, as becomes apparent at W-band frequencies where the spectrum is dominated by the axial g tensor (Fig. 5d). The CW EPR spectrum at X-band (Fig. 5b) reveals further features due to another radical (NH_2SO_3) with strongly anisotropic nitrogen hyperfine couplings; see also (*18, 19*).

MAS EPR experiments on this sample were performed at six values of the static field and at a temperature of 205 K. A typical spectrum at a single field position is shown in Fig. 7a; the sum of all six spectra in Fig. 7b. The spectrum is substantially narrowed but is not a single line. The apparent splitting might indicate a hyperfine coupling of 5–8 MHz, but a single-crystal proton ENDOR study of the SO_3^- center did not reveal such an isotropic coupling (*20*). Pulse ENDOR experiments on our own powder sample also do not suggest such an isotropic proton coupling. Furthermore, the splitting cannot be easily attributed to a coupling to a nitrogen nucleus in a neighbor molecule (at a distance of about 350 pm), because a triplet would then be expected in the spectrum. Note also that the spectrum does not exhibit the symmetry about its center that would be expected in an isotropic spectrum, although the deviation may not be significant at the given signal-to-noise ratio. At present we attribute the complex lineshape to the off-resonance effects discussed under Theory (see also Fig. 3).

Because of the difficulties in interpreting this spectrum, we have conducted a number of tests to check whether the signal is authentic. First, the MAS spectra at given observer positions characterized by the apparent g value $g_{app} = h\nu_{mw}/(\mu_B B_0)$ are reproducible, even if the mw frequency is slightly changed. Second, the signal is suppressed if reorientation angles are used that are significantly different from the theoretically required value of 120°. Third, the signal is also suppressed if the angle θ between rotation axis and static field direction is changed from the theoretically required value of 54.7° (Fig. 8). For these reasons we are quite confident that we have observed the MAS EPR spectrum of the SO_3^- center and that a spectrum of better quality could be obtained by improving the excitation bandwidth of the setup.

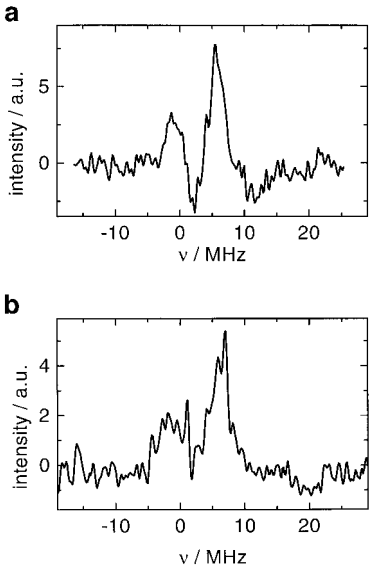

FIG. 7. MAS EPR on the SO_3^- anion radical in γ-irradiated sulfamic acid at $\nu_{rot} = 17$ kHz. (a) Spectrum obtained at a single observer position ($B_0 = 334.91$ mT, $\nu_{mw} = 9.388$ GHz, $t_{\pi/2} = 24$ ns). (b) Sum spectrum from six observer positions obtained by shifting the frequency scales to a common reference g value ($g = 2.0035$) and adding the spectra.

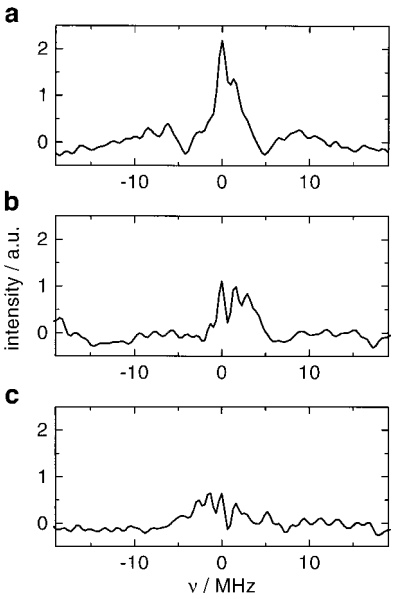

FIG. 8. Dependence of the MAS EPR spectrum of the SO_3^- anion radical in γ-irradiated sulfamic acid on the angle θ between the rotation axis and static field direction ($\nu_{mw} \sim 9.43$ GHz, $B_0 \sim 336$ mT, $\nu_{rot} \sim 17.1$ kHz, $t_{\pi/2} = 32$ ns). The static field was set to the value that ensured the same observer g value for all three measurements despite slightly different mw frequencies ($\Delta\nu_{mw} \leq 4.1$ MHz). (a) $\theta = 54.7°$ (magic angle). (b) $\theta = 60.7°$. (c) $\theta = 77°$.

CONCLUSION

It has been demonstrated that sample spinning in pulse EPR with rotation frequencies up to 17 kHz at temperatures down to 200 K is feasible without severely compromising the mw performance of the resonator. Pure absorption MAS EPR spectra can be obtained with a new phase cycle and exhibit narrower lines than the absolute-value spectra measured before. The residual line broadening in the MAS EPR spectrum of the E_1' center in γ-irradiated silica glass has been traced back to g strain by the observation of strain broadening in a high-field EPR spectrum of the same sample. Both theory and experiment show that the scope of applications for MAS EPR line narrowing is mainly restricted by the excitation bandwidth of the mw

pulses, which must be a significant fraction of the total width of the spectrum. With our current setup, the limit is expected at spectral widths of about 0.7 mT, as has been checked by observing MAS EPR signals of SO_3^- radicals in γ-irradiated sulfamic acid. If the currently available shortest $\pi/2$ pulse lengths of 3.6 ns (*17*) could be achieved with an MAS probehead, the limit could be extended to at least 3 mT. This should make it possible, for example, to separate the central lines of the nitrogen hyperfine triplet of nitroxides by their isotropic g values. While a broader application of MAS EPR thus requires further technological advances, current technology should be sufficient to extend the right-angle spinning experiments on transition metal ions by Sierra and Schweiger (*9*, *10*) to organic radicals by going from moderate to high rotation frequencies. Such experiments outside the linear regime for the reorientation angles are now in progress.

ACKNOWLEDGMENTS

The authors thank W. Lämmler and Prof. A. Schweiger (ETH Zürich) for help with the γ-irradiation of samples. Financial support from Deutsche Forschungsgemeinschaft within the Schwerpunktprogramm "Hochfeld-EPR in Biologie, Chemie und Physik," is gratefully acknowledged.

REFERENCES

1. E. R. Andrew, A. Bradbury, and R. G. Eades, *Nature* **183,** 1802 (1959).
2. I. Lowe, *Phys. Rev. Lett.* **2,** 285 (1959).
3. M. M. Maricq and J. S. Waugh, *J. Chem. Phys.* **79,** 3300 (1979).
4. C. Filip, S. Hafner, I. Schnell, D. E. Demco, and H. W. Spiess, *J. Chem. Phys.* **110,** 423 (1999).
5. A. Bax, N. M. Szevernyi, and G. E. Maciel, *J. Magn. Reson.* **52,** 147 (1983).
6. Z. Gan, *J. Am. Chem. Soc.* **114,** 8307 (1992).
7. M. Hubrich, C. Bauer, and H. W. Spiess, *Chem. Phys. Lett.* **273,** 259 (1997).
8. J. P. Hornak and J. H. Freed, *J. Magn. Reson.* **67,** 501 (1986).
9. G. A. Sierra and A. Schweiger, *Mol. Phys.* **95,** 973 (1998).
10. G. A. Sierra and A. Schweiger, *Rev. Sci. Instrum.* **68,** 1316 (1997).
11. M. Mehring, "High Resolution NMR Spectroscopy in Solids," Springer-Verlag, Berlin, 1983.
12. K. Schmidt-Rohr and H. W. Spiess, "Multidimensional Solid State NMR and Polymers," Academic Press, New York, 1994.
13. B. F. Chmelka and J. W. Zwanziger in "NMR Basic Principles and Progress," Vol. 33, p. 79, Springer-Verlag, Berlin, 1994.
14. K. Nakagawa, M. B. Candelaria, W. W. C. Chik, S. S. Eaton, and G. R. Eaton, *J. Magn. Reson.* **98,** 81 (1992).
15. R. A. Weeks and C. M. Nelson, *J. Am. Ceram. Soc.* **43,** 399 (1960).
16. B. T. Ghim, S. S. Eaton, G. R. Eaton, R. W. Quine, G. A. Rinard, and S. Pfenninger, *J. Magn. Reson. A* **115,** 230 (1995).
17. P. P. Borbat, R. H. Crepeau, and J. H. Freed, *J. Magn. Reson.* **127,** 155 (1997).
18. J. R. Rowlands and D. H. Whiffen, *Nature (London)* **193,** 61 (1962).
19. N. M. Atherton and J. R. Morton, *Nature (London)* **209,** 294 (1966).
20. N. M. Atherton, C. Oliva, E. J. Oliver, and D. M. Wylie, *J. Chem. Soc. Faraday Trans.* **83,** 3717 (1987).